Skeletonization Accelerated Solution of Crank-Nicolson Method for Solving Three-Dimensional Parabolic Equation

Hafiz Faiz Rasool, Chen Jun, Xiao-Min Pan*, and Xin-Qing Sheng

Center of Electromagnetic Simulation, School of Information and Electronics
Beijing Institute of Technology, Beijing, 100081, People's Republic of China
hafiz@bit.edu.cn, chenjun_11@foxmail.com, xsheng@bit.edu.cn, *xmpan@bit.edu.cn

Abstract ─ Parabolic equation models discretized with the finite difference method have been extensively studied for a long time. However, several explicit and implicit schemes exist in the literature. The advantage in explicit schemes is its simplicity, while its disadvantage is conditional stability. On the other hand, implicit schemes are unconditionally stable but require special treatment for a fast and accurate solution such as the Crank-Nicolson (CN) method. This method becomes computationally intensive for problems with dense meshes. The resulting matrix from the CN in two and three-dimensional cases requires high computational resources. This paper applies hierarchical interpolative factorization (HIF) to reduce the computational cost of the CN method. Numerical experiments are conducted to validate the proposed HIF acceleration.

Index Terms ─ Alternating direction implicit method, Crank-Nicolson method, hierarchical interpolative factorization, interpolative decomposition, Shur complement.

I. INTRODUCTION

The mathematical model of an electromagnetic problem is usually obtained in terms of partial differential equations (PDEs), integral equations, or integro-differential equations derived from Maxwell's equations. Numerical methods apply a sort of discretization which yields a linear system of algebraic equations (i.e., a matrix equation). The development of powerful computers and fast solution methods for linear systems like the multi-grid/multi-level methods has made the numerical solution of electromagnetic (EM) problems viable [1-3]. The extensive use of wireless communication speeds up the research in EM wave propagation in outdoor and indoor environments. The methods that have been traditionally used to model EM wave propagation in indoor environments (i.e., tunnels) are modal analysis, geometrical optics, and the parabolic equation (PE) approximation. The modal analysis method and the geometrical optics method both have unacceptable limitations and their applicability is limited to specific geometries. The parabolic equation method has been shown to provide a better balance between accuracy and efficiency [2].

Several numerical techniques are available to solve parabolic type equations such as the split-step parabolic equation (SSPE) method [1, 2, 6], the finite element method (FEM) [3], and the finite difference method (FDM) [4, 7, 15-17]. Among these, the finite-difference approaches are more popular because of their simplicity, flexibility, and capability to handle complex boundary conditions (BCs) at short-range propagation problems [8].

The Crank-Nicolson method has been widely used to model wave propagation in tunnels [15], [16]. The high computational cost is a serious obstacle to use the CN scheme in practice. The alternating direction implicit (ADI) methods were developed to address the problem of computational efficiency, but the application of these methods to the problems that vary in time or space encounters serious problems due to the necessity of initial and boundary conditions evaluation at the intermediate steps [7], [9], [10], [11-14]. The trade-off is the loss of accuracy.

In this paper, we improve the efficiency of the CN method by employing the HIF algorithm to make the methods based on 3DPE be potentially capable for problems that vary in time and space simultaneously. Several numerical experiments revealed substantial evidence that HIF can accurately approximate differential and integral operators in a variety of settings with high practical efficiency [18-22]. However, the performance of the HIF in accelerating the parabolic equation in our scenarios is still unclear. In order to answer the question and to find a remedy for the computational efficiency issue for the CN scheme, HIF fast solver has been employed. In order to establish a basis of comparison, the traditional rectangular waveguide model is chosen, as the analytical solution is available for this problem [16]. Secondly, a particular bended-waveguide model is considered to check the validity of the proposed method.

II. THE CN METHOD FOR 3DPE

A 3DPE can be obtained from the Helmholtz

Submitted On: March 27, 2020
Accepted On: June 5, 2020

https://doi.org/10.47037/2020.ACES.J.350905

equation in Cartesian coordinates (x, y, z) as [15]:

$$\left[\frac{\partial^2}{\partial x^2}+\frac{\partial^2}{\partial y^2}+\frac{\partial^2}{\partial z^2}+k_0^2\right]\varphi(x,y,z)=0, \qquad (1)$$

where φ is either the electric or magnetic field and $k_0 = 2\pi/\lambda$ is the free space wavenumber (λ is the wavelength). Assuming that, the direction of propagation is along the *z*-axis. A reduced function $\varphi(x,y,z) = e^{ik_0 z}u(x,y,z)$ is used to separate the rapidly varying phase term in Eq. (1) [15, 16]:

$$\left|\frac{\partial^2 u}{\partial z^2}\right| \ll k_0\left|\frac{\partial u}{\partial z}\right|, \qquad (2)$$

which physically corresponds to paraxial propagation, and substituting Eq. (2) into (1), a 3DPE can be obtained as [16]:

$$\frac{\partial u}{\partial z} = -\frac{1}{2ik_0}\left(\frac{\partial^2}{\partial x^2}+\frac{\partial^2}{\partial y^2}\right)u. \qquad (3)$$

In the following, Eq. (3) is numerically discretized by the CN method using a square grid (*xy*-plane), forwarding in the *z*-direction [4]. The grid points in *x*, *y*, and *z*-directions are denoted by ($i\Delta x$, $j\Delta y$, $n\Delta z$), where, $i = 0,1,2...N_x$, $j = 1,2,...N_y$, and $n = 1,2...N_z$. The transverse and longitudinal discretization's $\Delta x = \frac{x_{\max}}{N_x - 1}$, $\Delta y = \frac{y_{\max}}{N_y - 1}$, and $\Delta z = \frac{z_{\max}}{N_z - 1}$ are referred to as the incremental step sizes in *x*, *y*, and *z* directions, respectively. Consequently, the CN discretization of 3DPE mentioned in Eq. (3) can be written as:

$$r_x\left(u_{i+1,j}^{n+1}+u_{i-1,j}^{n+1}\right)+r_y\left(u_{i,j-1}^{n+1}+u_{i,j+1}^{n+1}\right)+\left(1-2r_x-2r_y\right)u_{i,j}^{n+1}$$
$$=-r_x\left(u_{i+1,j}^{n}+u_{i-1,j}^{n}\right)-r_y\left(u_{i,j-1}^{n}+u_{i,j+1}^{n}\right)+\left(1+2r_x+2r_y\right)u_{i,j}^{n}, \qquad (4)$$

where $r_x = \frac{\Delta z}{4ik_0\Delta x^2}$ and $r_y = \frac{\Delta z}{4ik_0\Delta y^2}$ are the mesh ratios.

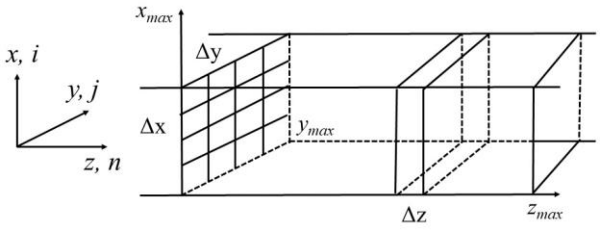

Fig. 1. The geometry of a three-dimensional rectangular waveguide model.

The two-dimensional (2D) cuts of the transverse plane are obtained along the propagation axis inside a rectangular tunnel's cross-section with perfectly conducting walls. The field is discretized at the plane of propagation into a mesh net and is evaluated at spatial steps along the direction of propagation, as illustrated in Fig. 1.

III. THE HIF ALGORITHM

Most recently, hierarchical interpolative factorization (HIF) has been proposed to efficiently and accurately solve a sparse matrix system of linear equations obtained by the discretization of finite difference or finite element methods in the form of $\mathbf{A}\cdot\boldsymbol{u} = \boldsymbol{f}$ [18]. The HIF factorization is based on the approximate decomposition where a recursive reduction strategy is employed to reduce the computational cost. An approximate representation of the original matrix is firstly obtained and then is used to compute the inverse. A threshold control to the reduction scheme is employed to reach the balance between the accuracy and the efficiency of the factorization. HIF works both for symmetric and general sparse matrices. In this work, we only focus on the HIF in terms of a symmetric matrix as the matrix arising from the CN scheme is symmetric. The recursive implementation of HIF is based on the commonly used octree [19]. According to the geometric coordinates, the HIF groups unknown degrees of freedom (DOFs) into the blocks using an octree available at https://github.com/klho/FLAM/. The HIF uses well known Shur complement and interpolative decomposition (ID) numerical tools for elimination and sparsification [18]. The elimination process is based on skeletonization which is divided into volumetric, face, and edge elimination. As discussed in Section II, a 3DPE is transformed into a series of 2D transverse planes propagating in the *z*-direction. So, for simplicity, we can solve a series of 2D problems to obtain the solution of a 3D problem. Consequently, the volumetric skeletonization is skipped in our discussion.

A. Overview of geometric factorization

In the solution process of partial differential equations (PDEs) and their application in a real problem, the partition of the domain is often necessary and convenient. Figures 2 (a)-(g) illustrate the idea of a domain partition, sparsification, and elimination processes based on Shur complement and skeletonization. Black dots correspond to the active DOFs for each level. The partition naturally induces a block representation of **A** proceeding in a hierarchical fashion. Figure 2 (a) shows the discretized domain transformation into a square grid and then splits the square domain into sixteen patches called "leaves" (they will be organized in a tree) [18]. During HIF factorization, the boundary points are selected as active points according to the skeletonization. As a result, the interior DOFs within all sixteen patches are eliminated, as shown in Fig. 2 (b). After the Shur complement sparsification, as discussed in [18], the interactions among the redundant interior DOFs are

represented by the active DOFs, namely, the boundary points on the edges of nearby patches. Figure 2 (c) shows the elimination of DOFs selected in Fig. 2 (b), placed on the edges of nearby cells. Merging cells and organizing the domain in a tree of patches, as shown in Fig. 2 (d). The alternative processes between Shur complement for cells and skeletonization for edges (Figs. 2 (e)-(f)), reduce the problem size into a reasonable size, as illustrated in Fig. 2 (g). This procedure is repeated for each cell up to the coarsest level based on hierarchical domain decomposition.

The resulting factorization allows the rapid application of the matrix inverse, which provides a fast direct solver or preconditioner, depending on the accuracy and specified relative precision (ε) of the ID. The relative precision of the ID is a specified positive real number used to control the accuracy of the HIF algorithm [18].

B. Skeletonization

Skeletonization figures out the redundant points according to the low-rank property of the matrix based on ID. To conduct skeletonization, the original symmetric matrix $\mathbf{A}$ is written as:

$$\mathbf{A} = \begin{bmatrix} \mathbf{A}_{CC} & \mathbf{A}_{CK}^{T} \\ \mathbf{A}_{CK} & \mathbf{A}_{KK} \end{bmatrix}, \tag{5}$$

where C collects the DOFs in a box at a given level and K denotes the rest of the DOFs. Generally, $\mathbf{A}_{CK}^{T}$ and $\mathbf{A}_{CK}$ are numerically low-rank matrices. HIF then conducts the ID on $\mathbf{A}_{CK}$ and obtains,

$$\begin{aligned} \mathbf{A}_{CK} &= \begin{bmatrix} \mathbf{A}_{RK} & \mathbf{A}_{SK}, \end{bmatrix} \approx \begin{bmatrix} \mathbf{T}_{C} \cdot \mathbf{A}_{SK} & \mathbf{A}_{SK} \end{bmatrix}, \\ \mathbf{A}_{CC} &= \begin{bmatrix} \mathbf{A}_{RR} & \mathbf{A}_{SR}^{T} \\ \mathbf{A}_{SR} & \mathbf{A}_{SS} \end{bmatrix}, \end{aligned} \tag{6}$$

where $\mathbf{T}_{C}$ is the interpolation matrix associated with the active unknowns, having indices $C = S \cup R$. Here, S denote the skeleton point set, and R is the redundant point set [18].

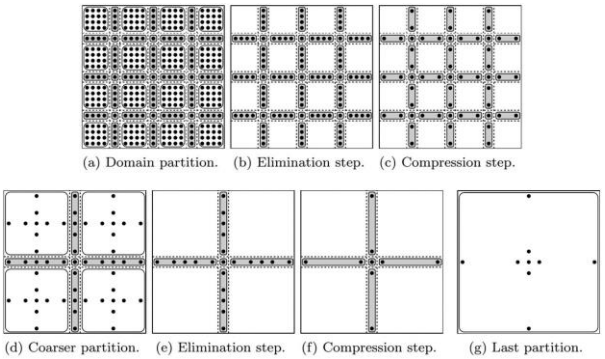

Fig. 2. Illustration of active DOFs at each level of HIF in the factorization process in a hierarchical fashion.

C. Schur complement sparsification

After the skeletonization, HIF obtains $\mathbf{A}_{RR}$ which represents self-interaction to the redundant point set R. By making use of the skeleton point set S, HIF eliminates the redundant points. Mathematically, $\mathbf{A}_{RR}$ is eliminated from $\mathbf{A}$ and a size-reduced form of $\mathbf{A}$ is obtained. When moving to a next active cell, the size-reduction of $\mathbf{A}$ takes place for the original matrix $\mathbf{A}$.

The detailed deduction and implementation, including a comprehensive accuracy control of the HIF algorithm, can be found in [18,19].

IV. SIMULATION RESULTS

Numerical simulations are performed on Intel (R) Core (TM) i3-4005U CPU @ 1.70 GHz, 8 GB RAM. First, the obtained results of the CN and ADI methods are verified via the analytical. The rectangular waveguide's cross-section dimensions are $(40\lambda \times 40\lambda)$ operating at 3 GHz frequency, where $\Delta x = \Delta y = 0.8\lambda$, and $\Delta z = 1\lambda$. A 2D Gaussian source is placed at the center of the waveguide at $(x_s, y_s, z_s) = (20\lambda, 20\lambda, 0)$ with a beamwidth of $\theta_{bw} = 4.34^{\circ}$, under Dirichlet boundary conditions applied on the walls of the rectangular waveguide.

We begin with the validation of the proposed method. Figures 3 (a-c) and (d-f) show the field distributions of a source with un-tilted $(x_{elv}, y_{elv}) = (0^{\circ}, 0^{\circ})$ and tilted $(x_{elv}, y_{elv}) = (-0.5^{\circ}, 0.5^{\circ})$ patterns in the *xy*-plane as a function of width-height variations at z = 100 m. As observed, CN and ADI methods agree with the analytical solution, where the error difference generated by both methods is about 1%. Figures 4 (a)-(c) show the resources used by the HIF factorization including factorization time (t_f), memory used in factorization (m_f), and the solution time (t_s), respectively. The overall solution time t_s includes the factorization construction time t_f and the time required for the HIF solver to evaluate the inverse of the given matrix.

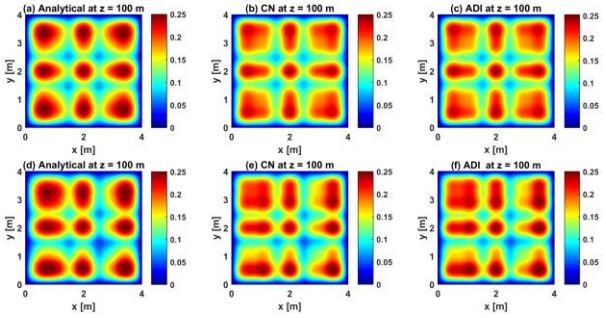

Fig. 3. The 2D field distribution as a function of width-height variations at z = 100 m by the analytical, CN,

and ADI methods, $\theta_{bw} = 4.34^\circ$, $\Delta x = \Delta y = 0.8\lambda$, and $\Delta z = 1\lambda$; TM polarization. (a-c): $(x_{elv}, y_{elv}) = (0^\circ, 0^\circ)$, (d-f): $(x_{elv}, y_{elv}) = (-0.5^\circ, 0.5^\circ)$.

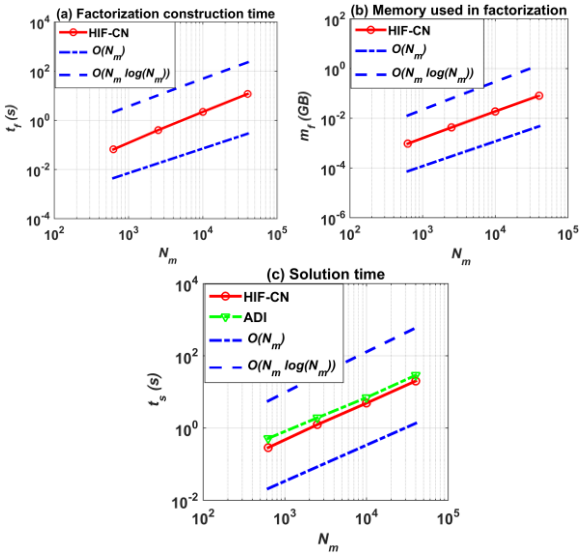

Fig. 4. Scaling results for the HIF-CN model for a PEC straight rectangular waveguide model. (a) Factorization construction time, (b) memory used in factorization, and (c) solution time of HIF-CN and ADI models, $\varepsilon = 10^{-9}$, and *occ* = 64. The data used in these figures are summarized in Table 1.

In this work, both the CN and ADI methods are designed to solve a matrix corresponding to the *xy*-plane. Hence, the overall matrix size corresponding to the *xy*-plane remains the same and can be compared for the given numerical tests. Here, N_m denotes the total number of DOFs solved by both models in the *xy*-plane corresponding to the tunnel's cross-section, while $O(N_m)$ and $O(N_m \log(N_m))$ are the extrapolated values which represent the reference scaling to estimate the efficiency of the algorithm. As the factorization is taking place on the *xy*-transverse plane, hence, t_f and m_f are only depending on the grid size. Furthermore, the size of the errors introduced by finite difference approximation of 3DPE can be controlled by the selection of the discretization intervals Δx and Δy. In order to avoid the aliasing effects, Nyquist's theorem restricts the transverse discretization's intervals $(\Delta x, \Delta y)$, to be less than 1.9λ [15]. The selection of the range increment Δz also depends on the accuracy requirements; it should be chosen as small as necessary to overcome numerical oscillation problems. It should be noted that the overall storage cost to store the field matrices by both models may also depend on the discretization points along the propagation axis, and similarly, the solution time t_s is also depending on: (i) the discretization points along the *z*-axis (ii) the time required for applying factorization *F* or F^{-1} (iii) the time required for solving multiple right-hand sides (iv) the time required for constructing octree, hence, $t_s > t_f$ [18]. The data used in these figures are summarized in Table 1.

Table 1: Factorization and matrix application results for the HIF-CN application in a straight rectangular waveguide model

ε	N_m	N_r	t_f (s)	t_s (s)	m_f (GB)	Error
10^{-6}	25^2	141	0.05	0.27	9.7e-4	1.3e-16
	50^2	651	0.30	1.21	4.3e-3	9.9e-8
	100^2	2775	2.1	3.91	1.8e-2	8.8e-7
	200^2	11439	10.4	18.4	7.9e-2	7.7e-7
10^{-9}	25^2	141	0.06	0.2	9.7e-4	4.6e-16
	50^2	651	0.40	1.24	4.3e-3	1.3e-10
	100^2	2775	2.2	4.8	1.9e-2	4.1e-10
	200^2	11439	11.8	20.0	8.2e-2	7.7e-10
10^{-12}	25^2	141	0.06	0.38	9.7e-4	5.4e-16
	50^2	651	0.46	1.58	4.4e-3	4.3e-14
	100^2	2775	2.6	6.2	1.9e-2	1.2e-12
	200^2	11439	18.6	21.2	8.6e-2	5.5e-13

The total cost of mf, tf, and ts is very close to $O(N_m)$. As can be seen in Table 1, the error generated by the HIF algorithm and the computational resources depends on the relative precision of ID (ε), as well as at the total number of DOFs. The remaining number of active DOFs (N_r) at the highest level are also shown for different N_m at tree occupancy parameter (*occ* = 64). The tree occupancy parameter (*occ*) shows the maximum number of points at each leaf node in a hyper-octree, as each nonempty node in hyper-octree is recursively subdivided until it contains at most *occ* points. As discussed in Section III, the HIF algorithm using a matrix sparsification technique called skeletonization, which facilitates the efficient inversion of the discretized operator obtained by the CN method and thus reduces the overall computational cost for the CN resulting matrix. It can be seen that for the given numerical example, the solution time of HIF-CN is sufficiently reduced when compared with the ADI method for the same problem size, as shown in Fig. 4 (c). The ADI methods are suitable for smooth and straight geometries, the application of theses method would result in the introduction of errors if the boundary conditions are varying rapidly, as significant energy coupling on the sloping terrain boundary between the two transverse directions can

occur within a single marching step. Thus, the marching of the vertical and horizontal field planes must be done simultaneously [7].

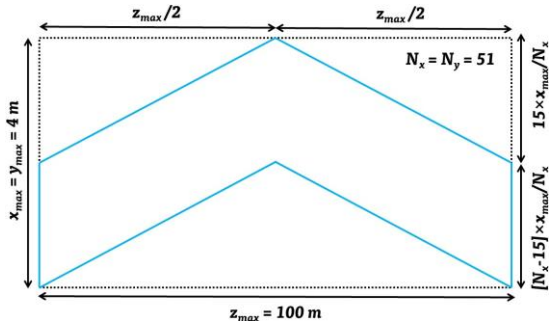

Fig. 5. The geometry of a typical bended-waveguide model.

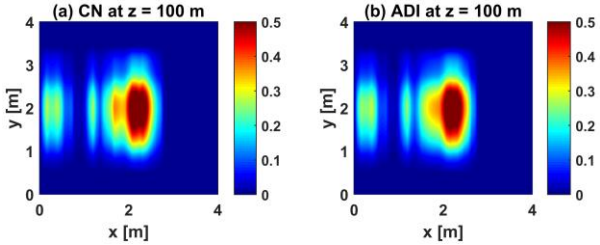

Fig. 6. The two-dimensional cross-sectional field distribution of the (a) CN and (b) ADI methods inside the bended-waveguide model as a function of width-height variation at z = 100 m.

The second test is related to the numerical solution of a bended-waveguide model, as illustrated in Fig. 5. Figures 6 (a) and (b) show the 2D field plots obtained at z = 100 m with un-tilted and tilted patterns of the radiating field. The 2D cuts of field plots are mostly good for visualization purposes. For precise validation, one-dimensional field plots are also obtained along the direction of propagation to check the accuracy of both models against the analytical solution, as shown in Fig. 7. The operational parameters are listed in Fig. 7 inset. The simulation results obtained from the proposed method for a bended-waveguide model are validated with the ADI method, as the analytical solution is not available for this problem in the available literature. A good agreement is observed between the two methods as most of the energy propagating through the simple geometries is contained inside the parabolic margin, the repeated application of the boundary condition at the inner fields converges the correct solution for the ADI method also. However, the overall accuracy would be reduced for the ADI method for modeling complex geometries or in the presence of an obstacle [9], [10].

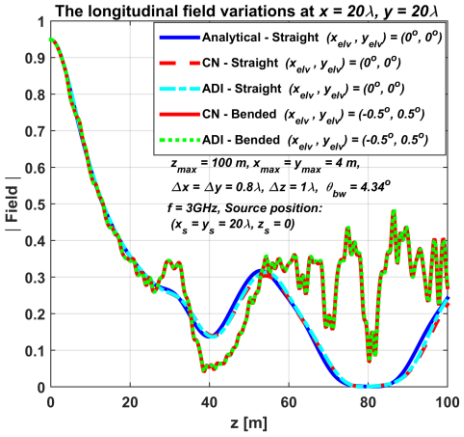

Fig. 7. The longitudinal field variations along the center of the bended-waveguide model according to the geometry shown in Fig. 5.

V. CONCLUSION

In this paper, the HIF based Crank-Nicolson (CN) method is proposed for the solution of a three-dimensional parabolic equation (3DPE). The traditional straight rectangular and particular bended-waveguide models are used for numerical tests. The simulation results are compared with the ADI method as well as against the analytical solution. The proposed work would help in reducing the computational cost of the CN method.

ACKNOWLEDGMENT

This work was supported in part by the National Natural Science Foundation of China (NSFC) under Grant No. 61771053, 61421001, the Key Laboratory for Information Science of Electromagnetic Waves under Grant EMW201908.

REFERENCES

[1] M. Levy, *Parabolic Equation Methods for Electromagnetic Wave Propagation*. London, IEE Institution of Electrical Engineers, 2000.

[2] G. Apaydin and L. Sevgi, *Radio Wave Propagation, and Parabolic Equation Modeling*. Wiley-IEEE Press, 2017.

[3] Ö. Ö. M. Kuzuoğlu, *MATLAB-based Finite Element Programming in Electromagnetic Modeling*. CRC Press, 2019.

[4] J. C. Strikwerda, *Finite Difference Schemes and Partial Differential Equations*. 2nd ed., Philadelphia, PA: SIAM, 2004.

[5] A. Hrovat, G. Kandus, and T. Javornik, "A survey of radio propagation modeling for tunnels," *IEEE Commun. Surveys Tuts.*, vol. 16, no. 2, pp. 658-669, 2nd Quarter, 2014.

[6] H. F. Rasool, X. M. Pan, and X. Q. Sheng, "A fourier split-step based wide-angle three-dimensional vector parabolic wave equation algorithm predicting the field strength over flat and irregular forest environments," *Applied Computational Electromagnetic Society Journal*, vol. 34, no. 6, pp. 874-881, June 2019.

[7] C. A. Zelly and C. C. Constantinou, "A three-dimensional parabolic equation applied to VHF/ UHF propagation over irregular terrain," *IEEE Trans. Antennas Propag*., vol. 47, pp. 1586-1596, Oct. 1999.

[8] Z. He, T. Su, H. C. Yin, and R. S. Chen, "Wave propagation modeling of tunnels in complex meteorological environments with parabolic equation," *IEEE Trans. Antennas Propag*., vol. 66, no. 12, pp. 6629-6634, 2018.

[9] P. Angot, J. Keating, and P. D. Minev, "A direction splitting algorithm for incompressible flow in complex geometries," *Computer Methods in Applied Mechanics and Engineering*, vol. 217-220, pp. 111-120, 2012.

[10] T. A. Dauzhenka and I. A. Gishkeluk, "Quasilinear heat equation in three dimensions and Stefan problem in permafrost soils in the frame of alternating directions finite difference scheme," *Proc. WCE*-London, UK, 2013.

[11] E. L. Tan, "Efficient algorithms for Crank-Nicolson-based finite-difference time-domain methods," *IEEE Transactions on Microwave Theory and Techniques*, vol. 56, no. 2, pp. 408-413, Feb. 2008.

[12] A. V. Londersele, D. D. Zutter, and D. V. Ginste, "Provably stable local application of Crank-Nicolson time integration to the FDTD method with nonuniform gridding and subgridding," *2018 Intl. App. Comp. Electromagnetics Society Symposium (ACES)*, Denver, CO, USA, Mar. 25-29, 2018.

[13] N. Feng, Y. Zhang, Q. Sun, J. Zhu, W. T. Joines, and Q. H. Liu, "An accurate 3-D CFS-PML based Crank–Nicolson FDTD method and its applications in low-frequency subsurface sensing," *IEEE Trans. Antennas Propag*., vol. 66, no. 6, pp. 2967-2975, June 2018.

[14] S. G. Garcia, T.-W. Lee, and S. C. Hagness, "On the accuracy of the ADI-FDTD method," *IEEE Antennas and Wave Propag. Letter*, vol. 1, pp. 31-34, 2002.

[15] R. Martelly and R. Janaswamy, "An ADI-PE approach for modeling radio transmission loss in tunnels," *IEEE Trans. Antennas Propag*., vol. 57, no. 6, pp. 1759-1770, June 2009.

[16] G. Apaydin and L. Sevgi, "Calibration of three-dimensional parabolic equation propagation models with the rectangular waveguide problem," *IEEE Antennas Propagat. Mag*., vol. 54, no. 6, pp. 102-116, Dec. 2012.

[17] X. Zhang, N. Sood, and C. D. Sarris, "Radio-wave propagation modeling in tunnels with a hybrid vector parabolic equation/waveguide mode theory method," *IEEE Trans. Antennas Propag.*, vol. 66, no. 12, pp. 6540-6551, June 2018.

[18] K. L. Ho and L. Ying, "Hierarchical interpolative factorization for elliptic operators: Differential equations," *Comm. Pure Appl. Math*., vol. 69, no. 8, 2016.

[19] K. L. Ho and L. Ying, "Hierarchical interpolative factorization for elliptic operators: Integral equations," *Comm. Pure Appl. Math*., vol. 69, pp. 1314-1353, no. 7, 2016.

[20] Y. N. Liu, X. M. Pan, and X. Q. Sheng, "Skeletonization accelerated MLFMA solution of volume integral equation for plasmonic structures," *IEEE Trans. Antennas Propag.*, vol. 66, no. 3, pp. 1590-1594, Mar. 2018.

[21] S. L. Huang, W. Song, Y. Z. Wang, Y. M. Wu, X. M. Pan, and X. Q. Sheng, "Efficient and accurate electromagnetic angular sweeping of rough surfaces by MPI parallel randomized low-rank decomposition," *IEEE Journal of Selected Topics in Applied Earth Observations and Remote Sensing*, vol. 13, no. 1, pp. 1752-1760, 2020.

[22] D. Wu, Y. N. Liu, Y. M. W. Wu, X. M. Pan, and X.-Q. Sheng, "Skeletonization improved calculation of electric fields by the impedance matrix of MoM," *IEEE Antennas and Wireless Propag. Lett*., Accepted, 2020.